**Astronomy**
**&**
**Astrophysics**

# Is GRB 050904 at z = 6.3 absorbed by dust?

G. Stratta[1,2], S. Gallerani[2], and R. Maiolino[2]

[1] ASI Science Data Center, via Galileo Galilei, 00044 Frascati, Italy
    e-mail: `giulia.stratta@asdc.asi.it`
[2] INAF – Osservatorio Astronomico di Roma, via di Frascati 33, 00040 Monte Porzio Catone, Italy

## ABSTRACT

Dust is an important tracer of chemical enrichment in primeval galaxies and it has also important implications for their evolution. So far, at $z > 6$, close to the reionization epoch, the presence of dust has only been firmly established in quasar host galaxies, which are rare objects associated with enormous star formation rates. The only non-quasar host galaxy, with modest star formation rate, for which dust extinction has been tentatively detected at these early cosmic epochs, is the host of gamma ray burst GRB 050904 at $z = 6.3$. However, the claim of dust extinction for this GRB has been debated in the past. We suggest that the discrepant results occur primarily because most of previous studies have not simultaneously investigated the X-ray to near-IR spectral energy distribution of this GRB. The difficulty with this burst is that the X-ray afterglow is dominated by strong flares at early times and is poorly monitored at late times. In addition, the Z band photometry, which is the most sensitive to dust extinction, has been found to be affected by strong systematics. In this paper we carefully re-analyze the Swift/XRT afterglow observations of this GRB, using extensive past studies of X-ray flare properties when computing the X-ray afterglow flux level and exploiting the recent reanalysis of the optical (UV rest frame) data of the same GRB. We extract the X-ray to optical/near-IR afterglow SED for the three epochs where the best spectral coverage is available: 0.47, 1.25, and 3.4 days after the trigger. A spectral power-law model has been fitted to the extracted SEDs. We discuss that no spectral breaks or chromatic temporal breaks are expected in the epochs of interest. To fit any UV rest-frame dust absorption, we tested the Small Magellanic Cloud (SMC) extinction curve, the mean extinction curve (MEC) found for a sample of QSO at $z > 4$ and its corresponding attenuation curve, the starburst attenuation curve, and the extinction curve consistent with a supernova dust origin (SN-type). The SMC extinction curve and the SN-type one provide good fit to the data at all epochs, with an average amount of dust absorption at $\lambda_{rest} = 3000$ Å of $A_{3000} = 0.25 \pm 0.07$ mag. These results indicate that the primeval galaxy at $z = 6.3$ hosting this GRB has already enriched its ISM with dust.

**Key words.** dust, extinction – gamma-ray burst: individual: GRB 050904

## 1. Introduction

The presence of dust at high redshifts ($z > 6$) is fundamental both for the formation and evolution of the stellar populations in early galaxies, as well as for their observability. High dust masses at $z > 6$ have been detected in the host galaxy of some powerful quasars, through detection of intense mm/submm (far-IR rest frame) dust emission (Bertoldi et al. 2003; Beelen et al. 2006; Wang et al. 2008). However, these powerful quasars are very rare objects, probably lying in extreme over-density peaks in the early universe, and hosted in extremely powerful starbursts, then forming stars at a rate higher than 1000 $M_\odot$/yr. It is important to understand whether dust is also present in less extreme galaxies at $z > 6$, which are more representative of the primeval galaxy population.

The main issue in the formation of dust in the early universe is the time scale for dust production mechanisms. In the local universe dust is mostly produced in the atmosphere of AGB stars, which require timescales ranging from a few 100 Myr to Gyrs to enrich the interstellar matter (ISM) with significant amounts of dust. These timescales may prevent young primeval galaxies in the early universe to have significant amounts of dust (but see also Valiante et al. 2009). Alternatively, dust production can occur in the ejecta of supernovae (SNe) (e.g., Todini & Ferrara 2001), which can enrich the ISM on a very short timescale, but which can also destroy dust through shocks (Bianchi & Schneider 2007; Nozawa et al. 2007).

If the dominant dust production mechanism changes over the cosmic epochs, this may result in a change in the dust properties (e.g., traced by the extinction curve) as a function of redshift. In the local universe and at low redshift, different systems are characterized by different extinction and attenuation curves. The Small Magellanic Cloud (SMC) extinction curve has been shown to reproduce the dust reddening of most quasars at $z < 2.2$ (Richards et al. 2003), while the effective reddening of galaxy spectra in the local Universe is generally modeled by using the attenuation law derived by Calzetti et al. (1994). The possibility that dust properties may evolve with redshift was first investigated by Maiolino et al. (2004) who analyzed the spectrum of the quasar SDSSJ1048+4637 at $z = 6.2$, finding that the reddening in this object is described better by an SN-type extinction curve (Todini & Ferrara 2001) than through the usually adopted SMC. A more extended study has been developed by Gallerani et al. (2010), who analyzed the optical-near infrared spectra of 33 quasars with redshifts $4.0 \leq z \leq 6.4$, finding that all of the reddened quasars require an extinction curve deviating from that of the SMC, with a tendency to flatten at $\lambda_{rest} < 2000$ Å. By performing a simultaneous fit of all reddened quasars in the sample, Gallerani et al. (2010) obtained a mean extinction curve (MEC) at $z > 4$, and the corresponding attenuation curve (hereafter called MEC$_{att}$). The change in extinction curve at $z > 4$ suggests that the dust properties at early epochs are different with respect to dust at intermediate and low redshifts, either because

of a different dust production mechanism (e.g., dominated by SNe instead of AGB stars) or because of different dust processing (e.g., stronger shocks destroying small grains).

High-$z$ GRBs provide additional opportunities to study the evolution of dust properties at high redshift (e.g., Stratta et al. 2007; Li et al. 2008; Zafar et al. 2010; Perley et al. 2009, 2010). In principle, this kind of studies may provide more stringent constraints on dust extinction curves relative to QSOs, since the intrinsic slope of their continuum can be inferred from the associated X-ray data, which are not affected by dust absorption. Moreover, GRBs have been discovered at redshifts greater than the ones of the most distant quasars, e.g., GRB 080913 at $z \sim 6.7$ (Greiner et al. 2009), and GRB 090423 at $z \sim 8.1$ (Salvaterra et al. 2009; Tanvir et al. 2009). Since (long) GRBs result from the death of (early) massive stars (e.g., Abel et al. 2002; Schneider et al. 2002; Woosley & Bloom 2006), they are expected to be detected at even earlier epochs. For these reasons GRBs are perfect candidates for investigating both the cosmic reionization process (Gallerani et al. 2008; Patel et al. 2010) and the evolution of the ISM properties through the cosmic epochs.

GRB 050904 was a very bright burst at $z = 6.29$ for which extensive multi-band afterglow follow-up has been performed (Cummings et al. 2005; Tagliaferri et al. 2005; Haislip et al. 2006; Price et al. 2006; Kawai et al. 2006; Boër et al. 2006). At the time of its discovery, GRB 050904 was the most distant GRB ever detected, and several works have been dedicated to broad band data analysis and modeling and to the study of the ISM in its host galaxy (e.g., Campana et al. 2007; Gendre et al. 2007). Dust extinction in GRB 050904 has been investigated by several authors, but with discordant results. By studying only the spectral energy distribution (SED) of the optical/near-IR data, assuming "standard" extinction curves (i.e. those of our Milky Way – MW – and for the two Magellanic Clouds – SMC, LMC –), several authors have found very low or zero values of dust extinction (Kann et al. 2007; Haislip et al. 2006; Perley et al. 2010). From wide-band spectral afterglow modeling, very low dust extinction values were inferred by Gou et al. (2007), assuming an MW extinction curve. Liang & Li (2009), in contrast, find evidence of non negligible dust extinction and a best-fit to the data assuming the extinction law computed by Li et al. (2008) with evidence of the 2175 Å absorption feature. By exploiting that X-ray emission is not affected by dust absorption, Stratta et al. (2007) have found evidence of dust extinction at a level comparable to what was found by Liang & Li (2009). This result was obtained both through the simultaneous optical to X-ray afterglow SED fitting at $T + 0.5$ day and also from the optical/near-IR SED fitting at later epochs. These authors also show that an extinction curve expected from dust produced by supernovae, such as the one found for a $z \sim 6$ QSO (e.g., Maiolino et al. 2004), provides a better fit to the data than the MW, LMC, SMC extinction curves and the Calzetti attenuation curves. Zafar et al. (2010) have published a new careful data reduction of the photometric data in the $Z$ band, which is one of the photometric points most sensitive to dust extinction and to different extinction curves. In their work, Zafar et al. (2010) find that, at $T + 0.47$ days, the $z$-band suppression is weaker than reported in the previous works and that in general the photometry calibration in this band is affected by systematic large uncertainties. By fitting the $zYJHK_s$ SED by assuming a power-law spectral model, leaving both the spectral index and normalization free to vary, and using any dust extinction curve (SMC and the same SN-origin extinction model used by Stratta et al. 2007), Zafar et al. (2010) find only marginal evidence of dust extinction at $T + 0.47$ days and no evidence at later epochs.

Given the importance of any confirmation of dust at such high redshifts, in this work we carefully revisit the global SED analysis for this burst. In particular, contrary to the majority of past works based on optical/near-IR data SED fitting alone, we exploit the X-ray afterglow emission of this burst to determine the spectral slope and normalization of the intrinsic, unabsorbed continuum. The difficulty with this burst is that the early X-ray afterglow is dominated by strong flare activity. X-ray flares are thought to be a distinct component than the afterglow one, possibly linked to the initial burst production mechanism (e.g., Falcone et al. 2007). We thus perform a new, detailed, and careful analysis of the X-ray afterglow of GRB 050904, devoting effort to estimating the X-ray flare afterglow contamination at the epochs of our interest. We take optical/near-IR data from the literature at $T + 0.47$, 1.25, and 3.4 days, where the photometric data in the $Z$ band is taken from the accurate reanalysis recently published by Zafar et al. (2010).

The results of our work are reported in Sect. 4 where we provide evidence that, at all three analyzed epochs, the optical and X-ray afterglow data of GRB 050904 are consistent with being extincted by dust, independent of the assumed extinction law model.

## 2. Swift/XRT data analysis

Swift/XRT data of GRB 050904 have been calibrated, filtered, and screened using the XRTDAS package included in the HEAsoft distribution (v6.9), as described in the XRT Software User's Guide[1]. The 0.3–10 keV light curve of this burst is flare-dominated at almost all epochs, at least up to one day after the trigger time ($T = 2005$ Sept. 5.0785 UT, Cummings et al. 2005). Given that the energy spectra of flares vary with time (e.g., Falcone et al. 2007), we take time-resolved spectral information into account when converting count-rates to energy fluxes. This procedure was performed with two methods. In the first one, we used the "xrtgrblc" v1.5 task. This task extracts the light curve from all the XRT observations (sequences) performed for this burst (Table 1), optimizing the source and background extraction regions and taking pile-up into account in a time-dependent manner. The conversion of the count-rates into flux units is performed on the basis of an energy spectra extraction in temporal bin with width that depends from the count-rate, and on the best-fit of each extracted spectrum assuming a double absorbed power-law spectral model, with one absorption component fixed at the Galactic value. Final fluxes are corrected for total absorption. In the second method, rather than extracting the spectrum in a count-rate dependent temporal region and fitting the power-law model to the data (as the "xrtgrblc" task does), the count-rate to flux conversion is performed by assuming the power-law photon indexes that best reproduce the observed hardness ratio and its evolution. This method is applied in the "burst analyzer" tool[2] (see more details in Evans et al. 2007, 2010). Comparing the light curves obtained with the two methods described above, we find overall agreement in terms of unabsorbed fluxes and spectral slopes, within errors (Fig. 1).

However, at late times ($t > T + 2$ days) the estimated flux is largely uncertain due to the very low flux level of the afterglow at this epoch: while the automatic time-dependent spectral analysis obtained with the "xrtgrblc" task and through the "burst analyzer" tool are extremely helpful for the first, bright part of the light curve, they may be not suitable for such faint

---

[1] http://swift.gsfc.nasa.gov/docs/swift/analysis/

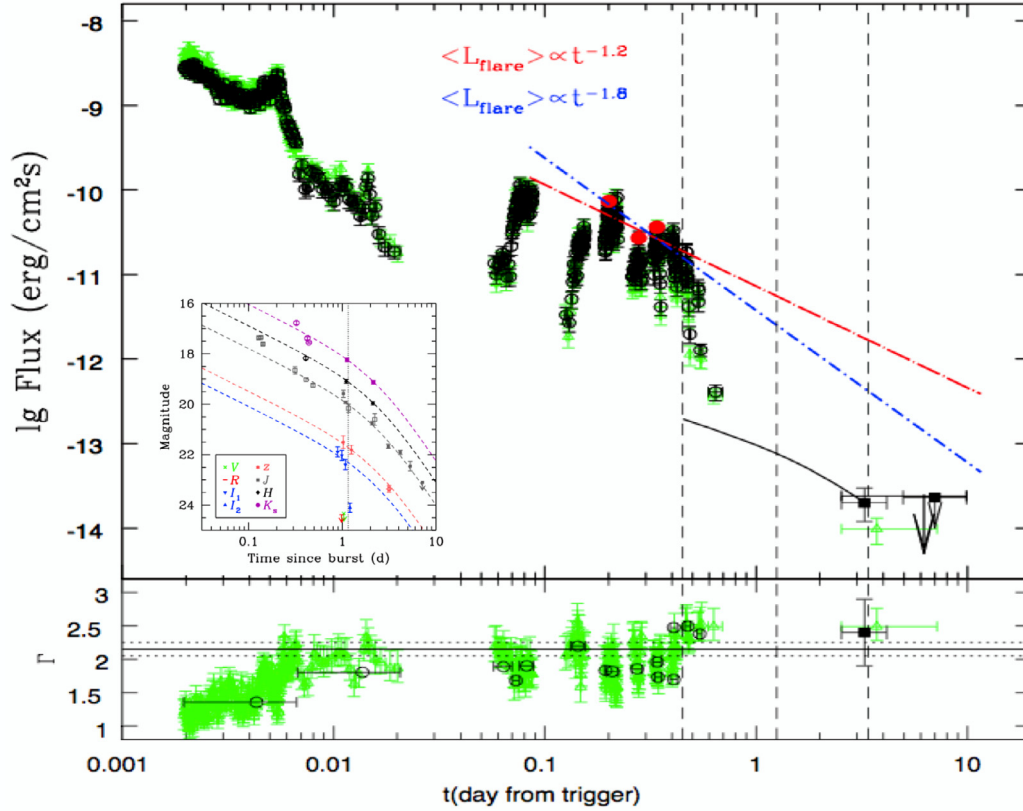[2] http://www.swift.ac.uk/burst_analyser/

**Fig. 1.** GRB 050904 X-ray afterglow unabsorbed flux as obtained from "xrtgrblc" task (open black circle) and from the "burst analyzer" tool by Evans et al. (2010) (green triangles). The black solid square at about 3.254 days after the burst trigger is the flux estimated with the stacking method discussed in the text and used in the temporal analysis. The solid line is the best-fit smoothed broken power-law model from the optical data from Tagliaferri et al. (2005) (see inserted panel). The dashed vertical lines indicate the three epochs at which the largest spectral optical coverage is available from the literature, namely $T + 0.47$, $T + 1.25$, and $T + 3.4$ days. The blue dot-short-dashed and red dot-long-dashed lines indicate the expected average flare intensity evolution with time, for two different decay rates predicted for late time flares (see Sect. 2.1 for more details). *The bottom panel* shows the X-ray photon index as a function of time obtained by both the "xrtgrblc" task (black circle) and the "burst analyzer" tool (green triangles), as well as the estimate obtained with the stacking method at about 3.4 days after the burst (black squares). Horizontal dashed line indicates the expected value at the epochs of our interest where $\nu_c < \nu_X$, for a synchrotron emission from an electron population with energy spectral index of $p \sim 2.1-2.5$, that is $\Gamma_X^{exp} = 2.15 \pm 0.10$.

**Table 1.** Swift/XRT observations of GRB 050904.

| Swift/XRT sequence ID | $T_{start}$ YYYY-MM-DD UT | $T_{end}$ YYYY-MM-DD UT | $\Delta T_{start}$ day | $\Delta T_{end}$ day |
|---|---|---|---|---|
| 00153514000 | 2005-09-04 02:01:26 | 2005-09-04 18:26:00 | 0.006738 | 0.6904 |
| 00153514001 | 2005-09-06 14:41:59 | 2005-09-06 18:38:56 | 2.535 | 2.699 |
| 00153514003 | 2005-09-07 00:29:33 | 2005-09-07 23:32:57 | 2.943 | 3.903 |
| 00153514004 | 2005-09-08 00:48:36 | 2005-09-08 05:42:51 | 3.956 | 4.16 |
| 00153514005 | 2005-09-09 00:52:08 | 2005-09-09 23:25:57 | 4.959 | 5.899 |
| 00153514006 | 2005-09-10 01:05:23 | 2005-09-11 06:17:58 | 5.968 | 7.185 |
| 00153514007 | 2005-09-13 01:03:19 | 2005-09-13 23:59:57 | 8.966 | 9.922 |

**Notes.** From left to right there are the Swift/XRT sequence (observation) identifying number, the start and end date of each sequence, and their corresponding distance in days from the burst trigger time. There are no XRT observations between 0.6904 and 2.535 days after the trigger.

detection levels. To accurately estimate the flux at late times we performed an alternative data analysis focused on this part of the light curve. We progressively stacked the observations starting from $T + 2.535$ days (sequence number 00153514001, see Table 1) up to the end of the XRT observation at $T + 9.922$ days.

The stacking of the cleaned event files was performed through the Xselect v2.4a software package, while the exposure maps were summed through the Ximage v4.5.1 software package. Since the source flux was fading, we find a maximum signal-to-noise ratio if we stop our stacking at $T + 4.16$ days (sequence

number 00153514004). Using the temporal range find above, we extracted the source and background energy spectrum from a circular region with a 10 pixel radius and an annulus region with an inner radius of 15 pixels and an outer radius of 30 pixels, respectively. By grouping the spectrum requiring a minimum of 5 counts per energy bin, we obtain a source energy spectrum with three energy bins. The model fitted to the obtained spectrum is an absorbed power-law model, with an absorption component fixed at the Galactic value in the direction of this burst ($4.6 \times 10^{20}$ cm$^{-2}$, Kalberla et al. 2005). Past results agree with no evidence of additional absorption at this epoch (e.g., Campana et al. 2007; Gendre et al. 2007). We find a best-fit photon index of $\Gamma = 2.4 \pm 0.5$ (68% confidence range) and a 0.3–10 keV unabsorbed flux of $(2.0^{+1.0}_{-0.8}) \times 10^{-14}$ erg cm$^{-2}$ s$^{-1}$ (68% confidence range). The obtained flux has been set at the photon-weighted mean epoch, that is at $T + 3.254$ days, with a start time of $T + 2.535$ days and an end time of $T + 4.160$ days (see Table 1).

The light curve we use in the following timing analysis is the one obtained from the "burst analyzer" tool since it provides a better temporal resolution of the spectral properties. For late-time observations we use the flux estimated with our faint source dedicated analysis as explained above.

## 2.1. X-ray flare analysis

To compare the SED of the optical afterglow with its X-ray counterpart, we need the X-ray flux level at those epochs with the best optical spectral coverage, which is at $T + 0.47$, $T + 1.25$ and $T + 3.4$ days (e.g., Zafar et al. 2010). At $T + 1.25$ days no XRT data are available (Table 1). At $T + 0.47$ days the X-ray light curve is flare-dominated, while the simultaneous afterglow optical counterpart does not show evidence of such intense flaring activity (Fig. 1). There is general consensus about considering flares to have a different origin than the afterglow (e.g., Falcone et al. 2007), therefore we need to estimate the X-ray afterglow flux level excluding the flares. Near $T + 3.4$ days there are XRT data centered at $T + 3.254$ days, thus requiring only a small temporal extrapolation.

Before proceeding to the X-ray afterglow flux extrapolation at the epochs of interest, we need to know whether late-time (i.e. after $\sim T + 0.5$ day) XRT data are still contaminated by flares or not. We know that the peak-to-continuum flux ratio $\Delta F/F$ of X-ray flares spans from $\sim$1 up to 1000 in some extreme cases (typically very early single flares): indeed, the median of $\Delta F/F$ computed over tens of GRBs and hundreds of flares (Chincarini et al. 2010) is about 4 and at late times is expected to be 1. Therefore, even if flare activity is present at late times for GRB 050904, we expect that the XRT data at $T + 3.254$ days would represent the afterglow flux level enhanced at worst by a factor of a few. However, in the following we provide some arguments that strongly support the idea that flare activity has deeply damped or ceased at late times for this burst.

Past studies have shown that the average X-ray flare peak luminosity $\langle L_{\text{flare}} \rangle$, corrected for the contribution of the underlying afterglow power-law component, decays with time as $\langle L_{\text{flare}} \rangle \propto t^{-\alpha}$, with $\alpha$ in the range 1.5–1.8 (Lazzati et al. 2008). Based on a larger sample, recently Margutti et al. (2011) have found that $\langle L_{\text{flare}} \rangle \propto t^{-2.7 \pm 0.1}$ for flares detected up to 1000 s after the burst onset (rest frame) and $\langle L_{\text{flare}} \rangle \propto t^{-1.2 \pm 0.1}$ at later times. Since at late time flares may be affected by a low signal-to-noise ratio[3], it has been argued that their unbiased intensity decay may be

steeper. For this reason, a joint fitting of early and late time flares has been performed, providing a unique decay index of $\alpha = 1.8$ (Bernardini et al. 2011).

We exploit these results to have an estimate of the expected flare intensity at late times for GRB 050904. The X-ray flux starting from about $T + 0.08$ days ($\sim T + 1000$ s rest frame) is completely dominated by flares so that the underlying continuum does not affect the peak flare evolution with time. In Fig. 1 we plot the average flare intensity evolution, with two possible decay rates, where the blue line marks $\alpha = 1.8$ and the red one marks $\alpha = 1.2$. Each power-law has been fitted to the three best-fit flare peaks found by Falcone et al. (2007) at late times (i.e., with $T + t_{\text{peak}} > 1000$ s in the rest frame) for this burst. The average flare evolution, computed assuming both $\alpha = 1.2$ and $\alpha = 1.8$, can trace the GRB 050904 flare peak intensity reasonably well up to about $T + 0.5$ days, with a preference for the shallower decay index (in agreement with past findings, see Lazzati et al. 2008, Margutti et al. 2011). If we assume that flare activity is still present at later times, the extrapolation overpredicts the observed fluxes by more than one order of magnitude. In addition, $\sim T + 0.5$ day marks a clear hard-to-soft spectral transition, as shown in the bottom panel of Fig. 1. Flares are spectrally harder than the underlying continuum (e.g., Margutti et al. 2011): the rather sharp spectral transition simultaneous to the flare peak intensity deviations from the average expected values is consistent with a scenario where flare activity has significantly damped, or ceased, at epochs later than $T + 0.5$ days. These findings enable us to consider the X-ray flux measure at $T + 3.254$ days with large confidence as representative of the flare unbiased afterglow flux level.

## 2.2. X-ray light curve modeling and flux extrapolation

To extrapolate the X-ray afterglow flux level at $T + 0.47$, $T + 1.25$ and $T + 3.4$ days, we need to assume a temporal model. Past broad band modelings of this burst have shown that data from radio to X-rays (e.g., Frail et al. 2006; Gou et al. 2007) are consistent with the fireball paradigms. The afterglow emission is commonly interpreted as synchrotron radiation emitted by a population of relativistic electrons (e.g., Meszaros & Rees 1997). The synchrotron cooling frequency (e.g., Sari et al. 1998) of GRB 050904, turns out to lie at energies below the optical range at the epochs of our interest (e.g., Kann et al. 2007; Frail et al. 2006), in agreement with the absence of any optical spectral variations at those epochs (e.g., Tagliaferri et al. 2005). Thus, X-rays and optical afterglow fluxes are expected to decay jointly, following the same light curve, with no spectral break between the two energy domains. Estimated values of the electron spectral index $p$ are within the range 2.1–2.5 (Frail et al. 2006; Gou et al. 2007; Zou et al. 2006; Chandra et al. 2010), providing an expected X-ray photon index $\Gamma_X^{\text{exp}} = \beta_X^{\text{exp}} + 1 = p/2 + 1$ in the range [2.05–2.25], that is consistent with our late time measure.

The optical afterglow light curve of GRB 050904 is well fitted by a smoothed broken power-law model between 0.1 and 10 days after the trigger, with best-fit decay indexes $\alpha_1 = 0.72 \pm 0.10$ and $\alpha_2 = 2.4 \pm 0.4$ and a break time at $t_b = 2.6 \pm 1.0$ days (Tagliaferri et al. 2005). Kann et al. (2007) quote $\alpha_1 = 0.85 \pm 0.08$ and similar $\alpha_2$ and $t_b$ fitting optical data from $T + 0.3$ days. The temporal break is achromatic, and therefore it has been interpreted as evidence for a jet with opening angle $\theta \sim 1/\Gamma(t_b)$, where $\Gamma(t_b)$ is the ejecta Lorentz factor at the epoch of the temporal break (e.g., Sari & Piran 1999).

We thus simply normalize the best-fit optical light curve model (from Tagliaferri et al. 2007) at the $T + 3.25$ day

---

[3] Indeed, Margutti et al. (2011) have shown that the evolution of the flare flux with time resembles the average detectability threshold one.

**Table 2.** Best-fit model parameters obtained for $\beta_{X,opt} = \beta_X \in [0.9; 1.9]$, i.e. $1\sigma$ interval of the X-ray energy spectral index value.

| Epoch | Extinction curve | $\beta_{X,opt}$ | $A_{3000}$ | $\tilde{\chi}^2_{BF}$ | $P(\tilde{\chi}^2 < \tilde{\chi}^2_{BF})$ |
|---|---|---|---|---|---|
| 0.47 days | **SMC** | $1.15^{+0.04}_{-0.04}$ | $0.36^{+0.01}_{-0.01}$ | **0.92** | **0.60** |
| | MEC | 1.19 | 0.69 | 1.68 | 0.81 |
| | Calzetti | 1.22 | 0.99 | 1.35 | 0.74 |
| | MEC$_{att}$ | 1.29 | 1.50 | 2.37 | 0.91 |
| | **SN-type** | $1.16^{+0.09}_{-0.09}$ | $0.51^{+0.03}_{-0.03}$ | **0.02** | **0.02** |
| 1.25 days | **SMC** | $1.11^{+0.11}_{-0.10}$ | $0.07^{+0.04}_{-0.02}$ | **0.07** | **0.02** |
| | MEC | $1.12^{+0.11}_{-0.11}$ | $0.14^{+0.06}_{-0.09}$ | 0.09 | 0.04 |
| | Calzetti | $1.13^{+0.11}_{-0.11}$ | $0.22^{+0.07}_{-0.17}$ | 0.08 | 0.03 |
| | MEC$_{att}$ | $1.15^{+0.11}_{-0.12}$ | $< 0.43$ | 0.11 | 0.04 |
| | **SN-type** | $1.11^{+0.11}_{-0.10}$ | $0.09^{+0.04}_{-0.03}$ | **0.11** | **0.04** |
| 3.4 days | **SMC** | $1.12^{+0.09}_{-0.08}$ | $0.19^{+0.02}_{-0.01}$ | **0.13** | **0.12** |
| | MEC | $1.15^{+0.08}_{-0.04}$ | $0.38^{+0.03}_{-0.07}$ | 0.30 | 0.26 |
| | Calzetti | $1.17^{+0.08}_{-0.18}$ | $0.57^{+0.02}_{-0.15}$ | 0.22 | 0.20 |
| | MEC$_{att}$ | $1.21^{+0.08}_{-0.08}$ | $0.90^{+0.04}_{-0.28}$ | 0.46 | 0.37 |
| | **SN-type** | $1.13^{+0.09}_{-0.09}$ | $0.27^{+0.03}_{-0.03}$ | **0.04** | **0.04** |

unabsorbed flux value (see Fig. 1). The X-ray flux extrapolations at $T + 0.47$, $T + 1.25$ days, and $T + 3.4$ days, are 0.03, 0.07, and 0.001 $\mu$Jy. We associated an uncertainty of 25% to the former two values and of about 50% to the last value, encompassing the uncertainty of the late X-ray flux measures.

## 3. Optical to X-ray spectral energy distribution

Starting from the results obtained in the previous section, we take from the literature the optical/near-IR data corrected for Galactic absorption at $T + 0.47$, 1.25, and 3.4 days, where the photometric data in the $Z$ band is taken from the accurate re-analysis recently published by Zafar et al. (2010), and we compare them with the simultaneous X-ray afterglow unabsorbed fluxes obtained in the previous section. We then fit a power-law spectral model to the data, setting the spectral index and normalization to the values obtained from X-ray afterglow. No spectral variation is expected during each epoch since $\nu_c < \nu_{X,opt}$ at these times (see Sect. 2.2). Given the large uncertainty affecting the X-ray photon index we have estimated at $T + 3.254$ days, we conservatively performed our analysis using both the expected ($\Gamma_X^{exp} = 2.15 \pm 0.10$, $\beta_X^{exp} = 1.15 \pm 0.10$) and the measured ($\Gamma_X = 2.4 \pm 0.5$, $\beta_X = 1.4 \pm 0.5$) X-ray photon indexes.

Figure 2 shows the obtained broad band SEDs at the three epochs. We note that our X-ray fluxes deviate significantly from those reported in Zafar et al. (2010) at $T + 0.47$ and $T + 1.25$ days. The latter discrepancy may be due to different light curve modeling and flux extrapolation. In Zafar et al. (2010) the X-ray light curve is modeled with a smoothed broken power-law, however parameter values are not reported, thus preventing further comparative studies.

To quantify the need for dust extinction and reddening, we fitted the data at each epoch with different extinction and attenuation curves. The question of whether dust reddening is better described by an extinction curve or by an attenuation law depends on the geometry of the system. For quasars, the simple dusty "screen" geometry applies, but for galaxies one has to consider that generally dust is mixed with the emitting sources (either stars or ionized gas). As a consequence, attenuation curves i.e. the ratio of the observed spectrum to the intrinsic total light emitted by the whole system before dust absorption, are likely more appropriate for galaxies. In the case of GRBs it is not

clear which geometry is more appropriate. The screen case is certainly more appropriate when the size of the emitting optical afterglow is smaller than the distribution of the dusty medium. However, the dust may well be the same as produced by the progenitor before the explosion. In this case the size of the dusty medium can be comparable to the one of the expanding afterglow, and an attenuation curve may be more appropriate. As a consequence, to describe dust reddening, we consider: the SMC extinction curve; the Calzetti attenuation law[4]; the MEC, and the corresponding attenuation curve MEC$_{att}$ (Gallerani et al. 2010) defined in Sect. 1; and finally the SN-type extinction curve proposed by Todini & Ferrara (2001), which reproduces the dust extinction observed in a BAL QSO at $z = 6.2$ (Maiolino et al. 2004; Gallerani et al. 2010). In Fig. 3, we plot the extinction and attenuation curves adopted in our analysis, normalized to $A_{3000}$, i.e., to the extinction value at the rest frame wavelength of $\lambda_{rest} = 3000$ Å.

We report the best-fit results for each extinction/attenuation curve and at each epoch in Tables 2–4, where we give the best-fit optical-to-X-ray spectral index $\beta_{X,opt}$ and $A_{3000}$, as well as the resulting best-fit reduced $\tilde{\chi}^2$ and the associated probability. Within each table we leave $\beta_{X,opt}$ free to vary in different intervals: $\beta_{X,opt} \in [0.9$–$1.9]$ in Table 2 and $\beta_{X,opt} \in [0.4$–$2.4]$ in Table 3, which correspond to the $1\sigma$ and $2\sigma$ errors on the measured $\beta_X$ at late times, respectively (see Sect. 2.1); $\beta_{X,opt} \in [1.05$–$1.25]$ in Table 4 is the range expected from synchrotron emission with $\nu_c < \nu_{X,opt}$ and $p \sim 2.1$–$2.5$ (see Sect. 2.2). The data in bold highlight the extinction/attenuation curve giving a good fit to the data ($P(\tilde{\chi}^2 < \tilde{\chi}^2_{BF}) < 68\%$) at all epochs.

In some cases the $\beta_{X,opt}$ best-fit value coincides with the lowest extreme of the interval considered. In these cases, we cannot compute the $1\sigma$ error on $A_{3000}$ and we only provide the interval within which this parameter is allowed to vary. Moreover, for some combinations of $\beta_{X,opt}$ intervals and extinction curves, the best-fit values are characterized by a $P(\tilde{\chi}^2 < \tilde{\chi}^2_{BF}) > 68\%$; in these cases, we only provide the best-fit values.

---

[4] It has been shown that the Calzetti law is the result of the attenuation by a medium with an SMC-type dust (Gordon et al. 1997; Inoue 2005). But see also Panuzzo et al. (2007) and Pierini et al. (2004).

**Table 3.** Best-fit parameters obtained for $\beta_{\rm X,opt} = \beta_{\rm X} \in [0.4; 2.4]$, i.e., $2\sigma$ interval of the X-ray energy spectral index value.

| Epoch | Extinction curve | $\beta_{\rm X,opt}$ | $A_{3000}$ | $\tilde{\chi}^2_{\rm BF}$ | $P(\tilde{\chi}^2 < \tilde{\chi}^2_{\rm BF})$ |
|---|---|---|---|---|---|
| 0.47 days | **SMC** | $1.15^{+0.04}_{-0.04}$ | $0.36^{+0.01}_{-0.01}$ | **0.92** | **0.60** |
|  | MEC | 1.19 | 0.69 | 1.68 | 0.81 |
|  | Calzetti | 1.22 | 0.10 | 1.35 | 0.74 |
|  | MEC$_{\rm att}$ | 1.29 | 1.50 | 2.37 | 0.91 |
|  | **SN-type** | $1.16^{+0.09}_{-0.09}$ | $0.51^{+0.03}_{-0.03}$ | **0.02** | **0.02** |
| 1.25 days | **SMC** | $1.11^{+0.11}_{-0.11}$ | $0.07^{+0.06}_{-0.02}$ | **0.07** | **0.02** |
|  | MEC | $1.12^{+0.11}_{-0.11}$ | $0.14^{+0.06}_{-0.09}$ | 0.09 | 0.04 |
|  | Calzetti | $1.13^{+0.11}_{-0.11}$ | $0.22^{+0.07}_{-0.17}$ | 0.08 | 0.03 |
|  | MEC$_{\rm att}$ | $1.15^{+0.11}_{-0.12}$ | $< 0.43$ | 0.11 | 0.04 |
|  | **SN-type** | $1.11^{+0.11}_{-0.10}$ | $0.09^{+0.04}_{-0.03}$ | **0.11** | **0.04** |
| 3.4 days | **SMC** | $1.12^{+0.09}_{-0.08}$ | $0.19^{+0.02}_{-0.01}$ | **0.13** | **0.12** |
|  | MEC | $1.15^{+0.08}_{-0.04}$ | $0.38^{+0.03}_{-0.07}$ | 0.30 | 0.26 |
|  | Calzetti | $1.17^{+0.08}_{-0.18}$ | $0.57^{+0.02}_{-0.15}$ | 0.22 | 0.20 |
|  | MEC$_{\rm att}$ | $1.21^{+0.08}_{-0.08}$ | $0.90^{+0.04}_{-0.28}$ | 0.46 | 0.37 |
|  | **SN-type** | $1.13^{+0.09}_{-0.09}$ | $0.27^{+0.03}_{-0.03}$ | **0.04** | **0.04** |

**Table 4.** Best-fit model parameters obtained for $\beta_{\rm X,opt} = \beta_{\rm X} \in [1.05; 1.25]$ i.e., the interval of the theoretically expected X-ray photon index for an electron spectral index $p \sim 2.1-2.5$ and $\nu_{\rm c} < \nu_{\rm X}$.

| Epoch | Extinction curve | $\beta_{\rm X,opt}$ | $A_{3000}$ | $\tilde{\chi}^2_{\rm BF}$ | $P(\tilde{\chi}^2 < \tilde{\chi}^2_{\rm BF})$ |
|---|---|---|---|---|---|
| 0.47 days | **SMC** | $1.15^{+0.04}_{-0.04}$ | $0.36^{+0.01}_{-0.01}$ | **0.92** | **0.60** |
|  | MEC | 1.19 | 0.69 | 1.68 | 0.81 |
|  | Calzetti | 1.22 | 0.99 | 1.35 | 0.74 |
|  | MEC$_{\rm att}$ | 1.25 | 1.39 | 2.60 | 0.92 |
|  | **SN-type** | $1.16^{+0.09}_{-0.09}$ | $0.51^{+0.03}_{-0.03}$ | **0.02** | **0.02** |
| 1.25 days | **SMC** | $1.11^{+0.11}_{-0.11}$ | $0.09^{+0.01}_{-0.02}$ | **0.07** | **0.02** |
|  | MEC | $1.12^{+0.11}_{-0.11}$ | $0.14^{+0.06}_{-0.01}$ | 0.09 | 0.04 |
|  | Calzetti | $1.13^{+0.09}_{-0.08}$ | $0.22^{+0.07}_{-0.08}$ | 0.08 | 0.03 |
|  | MEC$_{\rm att}$ | $1.15^{+0.11}_{-0.12}$ | $0.42^{+0.02}_{-0.31}$ | 0.11 | 0.04 |
|  | **SN-type** | $1.11^{+0.11}_{-0.06}$ | $0.11^{+0.02}_{-0.02}$ | **0.11** | **0.04** |
| 3.4 days | **SMC** | $1.12^{+0.09}_{-0.08}$ | $0.19^{+0.02}_{-0.01}$ | **0.13** | **0.12** |
|  | MEC | $1.15^{+0.08}_{-0.08}$ | $0.38^{+0.03}_{-0.07}$ | 0.30 | 0.26 |
|  | Calzetti | $1.17^{+0.08}_{-0.06}$ | $0.57^{+0.02}_{-0.16}$ | 0.22 | 0.20 |
|  | MEC$_{\rm att}$ | $1.21^{+0.05}_{-0.08}$ | $0.90^{+0.06}_{-0.28}$ | 0.46 | 0.37 |
|  | **SN-type** | $1.13^{+0.09}_{-0.08}$ | $0.27^{+0.03}_{-0.02}$ | **0.04** | **0.04** |

# 4. Results

Tables 2 to 4 show that, regardless of the interval adopted for $\beta_{\rm X,opt}$ and taking only the best-fit with $P(\tilde{\chi}^2 < \tilde{\chi}^2_{\rm BF}) < 68\%$ into account, all epochs require dust extinction. The SMC and SN-type extinction curves provide a good fit to the data at all the three analyzed epochs (Fig. 2).

At $T + 0.47$ days and at $T + 1.25$ days the obtained extinction values are systematically higher and lower, respectively, than those obtained at $T + 3.4$ days. Since such an evolution with time has no physical explanation, we interpret these discrepancies as the result of the systematics affecting the optical data reduction (see Zafar et al. 2010). By averaging the results obtained assuming the SMC and the SN-type extinction curve over all epochs, the amount of dust absorption at $\lambda_{\rm rest} = 3000$ Å is

at a level of $\langle A_{3000} \rangle = 0.25 \pm 0.07$ mag where the uncertainty (68% confidence range) takes our ignorance on the true extinction curve into account. The average best-fit optical to X-ray spectral index, independent of its initial fixed range (Tables 2–4), is $\langle \beta_{\rm X,opt} \rangle = 1.13 \pm 0.22$, which is nicely consistent with the range of values expected from past broad band modeling of this burst, which is $p/2$ with the electron spectral index in the range $p \sim 2.1-2.5$ (Frail et al. 2006; Gou et al. 2007; Zou et al. 2006; Chandra et al. 2010).

We find that the average properties of X-ray flares (Margutti et al. 2011; Bernardini et al. 2011; Chincarini et al. 2010) provide convincing indications that flare activity is strongly damped or has ceased at late times for GRB 050904. We estimate the transition from flare-dominated to afterglow-dominated X-ray flux at about $T + 0.5$ day, where the expected average flare peak
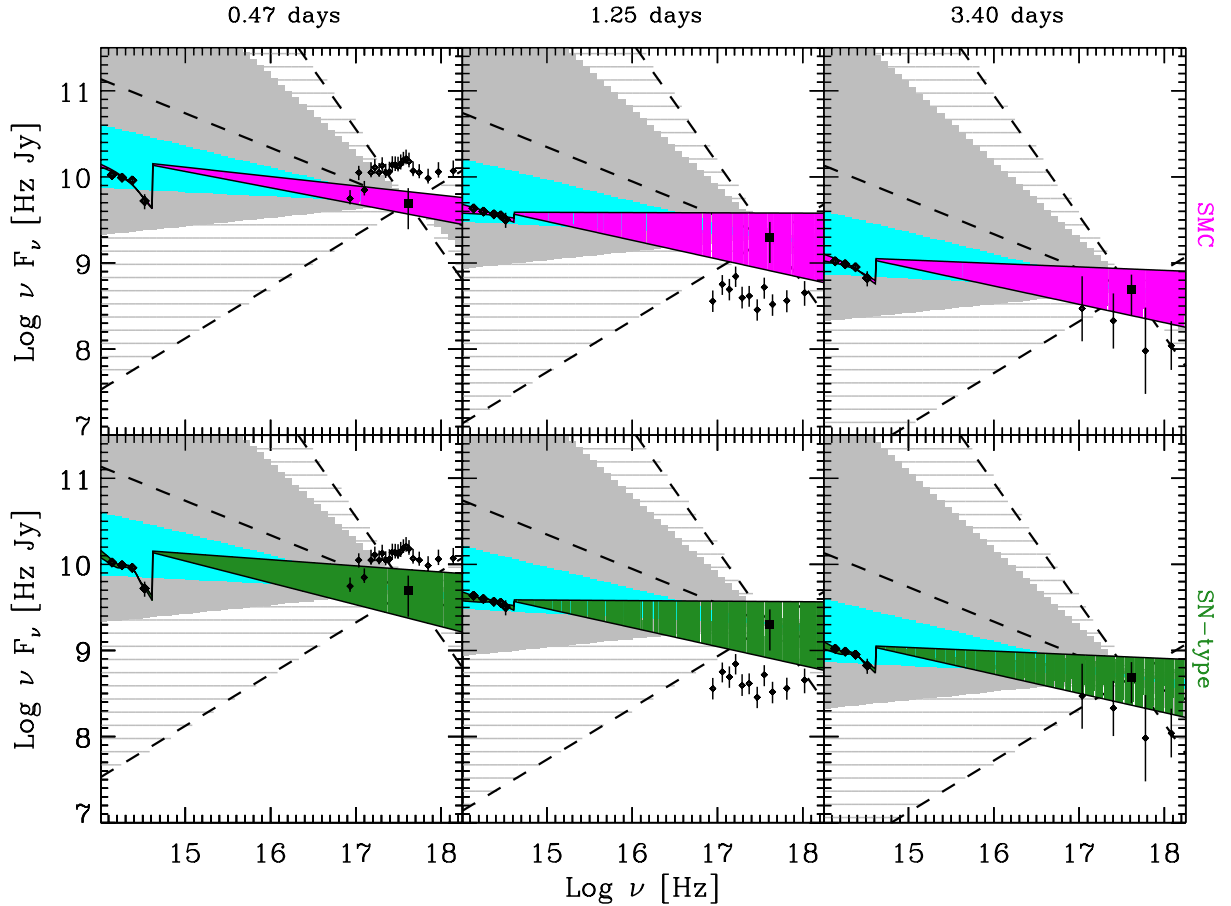
**Fig. 2.** Optical to X-ray SED at 0.47, 1.25 and 3.4 days after the burst trigger (*from left to right*) and fitted using the two extinction curves that provide excellent fit at all epochs, that is, the SMC and the SN-type (*from top to bottom*). Squares show the X-ray flux obtained by our analysis while diamonds are the fluxes by Zafar et al. (2010). The hatched area (delimited by dashed lines) indicates the range of intrinsic power-laws consistent with the $\pm 2\sigma$ uncertainty on $\beta_X$. The dashed line in the middle shows the power-law resulting from the best-fit slope to the X-ray data at late epochs ($\beta_X = 1.4$). The gray shaded areas show the range of intrinsic power-laws consistent with the $\pm 1\sigma$ uncertainty on $\beta_X$. The cyan shaded areas show the the power-laws expected from synchrotron emission (for an electron spectral index $p \sim 2.1-2.5$ and $\nu_c < \nu_{X,opt}$). The colored areas show the optical to X-ray SED best-fit assuming a power-law model with index free to vary within the range $\beta_X \pm 2\sigma$ (Table 3).

intensity starts to overpredict the observed fluxes and when an abrupt hard-to-soft spectral transition is observed (Fig. 1). The X-ray flux measure at $T + 3.254$ days is more than one order of magnitude lower than the expected flare intensity, therefore is likely representative of the flare-unbiased afterglow flux level. Results quoted in Tables 2–4 were obtained by extrapolating the X-ray afterglow at the three epochs where best optical/near-IR spectral coverage is available, normalizing the best-fit temporal model obtained at optical wavelengths (Tagliaferri et al. 2005) at the X-ray unabsorbed flux value measured at $T + 3.254$ days (Fig. 1).

It may be argued that several GRBs show that X-ray and optical afterglow light curves do not decay with the same behavior (e.g., Panaitescu et al. 2006). However, even though there is also a non negligible fraction of GRBs for which the optical and X-ray emission decay jointly (e.g., Oates et al. 2011), GRB 050904 is one of the few bursts for which a broad band modeling was feasible from radio to X-rays. In particular, it has been found that GRB 050904 data are generally consistent with fireball paradigms, with the synchrotron cooling frequency below the optical range at the epochs of interest (e.g., Frail et al. 2006), thus supporting our assumption on the optical and X-ray temporal behavior. In addition, results for dust extinction at $T + 0.47$

and $T + 1.25$ days are on average consistent with the $A_{3000}$ values obtained at $T + 3.4$ days, when the Swift/XRT observations are available at $T + 3.254$ days, and thus where flux extrapolation depends little on the assumed temporal model. At $T + 3.4$ days, the extracted X-ray to optical SED shows clear evidence of dust extinction, with $A_{3000}$ in the range that goes from 0.2 to 0.9 mag, depending on the assumed dust recipe (Tables 2–4).

These results indicate, beyond a doubt, that the primeval galaxy at $z = 6.3$ hosting this GRB has already enriched its ISM with dust. However, while the presence of dust attenuating the GRB 050904 optical afterglow at any epoch is firmly established, the type of extinction/attenuation curve is not well constrained, although we find that only the SMC and SN-type extinction curves provide a good fit to the data ($P(\tilde{\chi}^2 < \tilde{\chi}^2_{BF}) < 68\%$) at all epochs (Fig. 2).

## 5. Summary and conclusions

We reanalyzed the afterglow of GRB 050904 at $z = 6.3$ at those epochs where the best spectral coverage is available in the optical/near-IR range (UV rest frame), namely at 0.47, 1.25, and 3.4 days after the trigger, by fitting the simultaneous optical/near-IR and X-ray SED. In this work, we exploited the
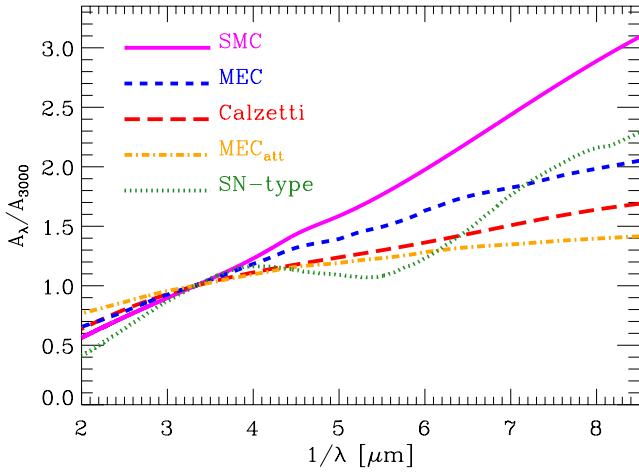
**Fig. 3.** Extinction and attenuation curves adopted in our analysis, normalized to the extinction value at the rest frame wavelength of $\lambda_{rest} = 3000$ Å.

recent reanalysis done by Zafar et al. (2010) on $Z$-band data, which are the most sensitive to dust reddening for this burst. We analyzed the Swift/XRT data of GRB 050904, taking special care to estimate the flare unbiased afterglow flux level at the epochs of interest and to extrapolate the flux where no data are available.

A spectral power-law model was fitted to the extracted SEDs, setting the spectral index and normalization at the dust-unbiased X-ray emission values. No spectral breaks or chromatic temporal breaks between X-rays and optical wavelengths are expected at these epochs, according to past broad band modeling results for this burst (e.g., Frail et al. 2006; Gou et al. 2007). Indeed, this predicts that the synchrotron cooling frequency $\nu_c$ is already below the optical range at the time of interest, thus an identical afterglow decay law at X-ray and optical wavelengths is expected.

We investigated any presence of dust extinction in the GRB afterglow by using the SMC extinction curve and the Calzetti attenuation law. We also used the MEC at $4.0 < z < 6.4$ inferred by Gallerani et al. (2010) from the analysis of 33 quasars, and the associated attenuation curve (MEC$_{att}$). The SN-type extinction curve, proposed by Todini & Ferrara (2001), which reproduces the dust extinction observed in a BAL QSO at $z = 6.2$ (Maiolino et al. 2004; Gallerani et al. 2010) was also tested.

From a simultaneous fit of the rest frame UV to X-ray SED, we find clear evidence of dust absorption at all epochs. The SMC and SN-type extinction curves provide good fits at all epochs, with an average value of dust extinction of $0.25 \pm 0.07$ mag at $\lambda_{rest} = 3000$ Å. At $T + 3.4$ days where nearly simultaneous X-ray and optical data are available, thus where X-ray temporal extrapolation weakly depends on the assumed model, the extracted X-ray to optical SED shows clear evidence of dust extinction, with $A_{3000}$ in the range that goes from 0.2 to 0.9 mag, depending on the assumed dust recipe (Tables 2–4).

Our findings indicate that the primeval star-forming galaxy at $z = 6.3$ hosting this GRB has already enriched its ISM with dust. The type of extinction/attenuation curve is not well constrained by the data, although we find that only the SMC and SN-type extinction curves provide good fit to the data at all epochs.

We emphasize that our results were obtained from a simultaneous optical to X-ray SED fitting, while most of the previous studies were performed on the optical/near-IR SED alone. Our method strongly benefits from the information from past broad band modeling and from the X-ray afterglow flux normalization level and spectral slope at 3.25 days after the trigger, when we demonstrated that the flare activity has very likely ceased.

## References

Abel, T., Bryan, G. L., & Norman, M. L. 2002, Science, 295, 93
Beelen, A., Cox, P., Benford, D. J., et al. 2006, ApJ, 642, 694
Bernardini, M. G., Margutti, R., Chincarini, G., Guidorzi, C., & Mao, J. 2011, A&A, 526, A27
Bertoldi, F., Carilli, C. L., Cox, P., et al. 2003, A&A, 406, L55
Bianchi, S., & Schneider, R. 2007, MNRAS, 378, 973
Boër, M., Atteia, J. L., Damerdji, Y., et al. 2006, ApJ, 638, L71
Calzetti, D., Kinney, A. L., & Storchi-Bergmann, T. 1994, ApJ, 429, 582
Campana, S., Lazzati, D., Ripamonti, E., et al. 2007, ApJ, 654, L17
Chandra, P., Frail, D. A., Fox, D., et al. 2010, ApJ, 712, L31
Chincarini, G., Mao, J., Margutti, R., et al. 2010, MNRAS, 406, 2113
Cummings, J., Angelini, L., Barthelmy, S., et al. 2005, GRB Coordinates Network, 3910, 1
Evans, P. A., Beardmore, A. P., Page, K. L., et al. 2007, A&A, 469, 379
Evans, P. A., Willingale, R., Osborne, J. P., et al. 2010, A&A, 519, A102
Falcone, A. D., Morris, D., Racusin, J., et al. 2007, ApJ, 671, 1921
Frail, D. A., Cameron, P. B., Kasliwal, M., et al. 2006, ApJ, 646, L99
Gallerani, S., Salvaterra, R., Ferrara, A., & Choudhury, T. R. 2008, MNRAS, 388, L84
Gallerani, S., Maiolino, R., Juarez, Y., et al. 2010, A&A, 523, A85
Gendre, B., Galli, A., Corsi, A., et al. 2007, A&A, 462, 565
Gordon, K. D., Calzetti, D., & Witt, A. N. 1997, ApJ, 487, 625
Gou, L., Fox, D. B., & Mészáros, P. 2007, ApJ, 668, 1083
Greiner, J., Clemens, C., Krühler, T., et al. 2009, A&A, 498, 89
Haislip, J. B., Nysewander, M. C., Reichart, D. E., et al. 2006, Nature, 440, 181
Inoue, A. K. 2005, MNRAS, 359, 171
Kann, D. A., Masetti, N., & Klose, S. 2007, AJ, 133, 1187
Kawai, N., Kosugi, G., Aoki, K., et al. 2006, Nature, 440, 184
Lazzati, D., Perna, R., & Begelman, M. C. 2008, MNRAS, 388, L15
Li, A., Liang, S. L., Kann, D. A., et al. 2008, ApJ, 685, 1046
Liang, S. L., & Li, A. 2009, ApJ, 690, L56
Maiolino, R., Schneider, R., Oliva, E., et al. 2004, Nature, 431, 533
Margutti, R., Bernardini, G., Barniol Duran, R., et al. 2011, MNRAS, 410, 1064
Meszaros, P., & Rees, M. J. 1997, ApJ, 476, 232
Nozawa, T., Kozasa, T., Habe, A., et al. 2007, ApJ, 666, 955
Oates, S. R., Page, M. J., Schady, P., et al. 2011, MNRAS, 412, 561
Panaitescu, A., Mészáros, P., Burrows, D., et al. 2006, MNRAS, 369, 2059
Panuzzo, P., Granato, G. L., Buat, V., et al. 2007, MNRAS, 375, 640
Patel, M., Warren, S. J., Mortlock, D. J., & Fynbo, J. P. U. 2010, A&A, 512, L3
Perley, D. A., Cenko, S. B., Bloom, J. S., et al. 2009, AJ, 138, 1690
Perley, D. A., Bloom, J. S., Klein, C. R., et al. 2010, MNRAS, 406, 2473
Pierini, D., Maraston, C., Bender, R., & Witt, A. N. 2004, MNRAS, 347, 1
Price, P. A., Cowie, L. L., Minezaki, T., et al. 2006, ApJ, 645, 851
Richards, G. T., Hall, P. B., Vanden Berk, D. E., et al. 2003, AJ, 126, 1131
Salvaterra, R., Della Valle, M., Campana, S., et al. 2009, Nature, 461, 1258
Sari, R., & Piran, T. 1999, ApJ, 517, L109
Sari, R., Piran, T., & Narayan, R. 1998, ApJ, 497, L17
Schneider, R., Ferrara, A., Natarajan, P., & Omukai, K. 2002, ApJ, 571, 30
Stratta, G., Maiolino, R., Fiore, F., & D'Elia, V. 2007, ApJ, 661, L9
Tagliaferri, G., Antonelli, L. A., Chincarini, G., et al. 2005, A&A, 443, L1
Tanvir, N. R., Fox, D. B., Levan, A. J., et al. 2009, Nature, 461, 1254
Todini, P., & Ferrara, A. 2001, MNRAS, 325, 726
Valiante, R., Schneider, R., Bianchi, S., & Andersen, A. C. 2009, MNRAS, 397, 1661
Wang, R., Carilli, C. L., Wagg, J., et al. 2008, ApJ, 687, 848
Woosley, S. E., & Bloom, J. S. 2006, ARA&A, 44, 507
Zafar, T., Watson, D. J., Malesani, D., et al. 2010, A&A, 515, A94
Zou, Y. C., Dai, Z. G., & Xu, D. 2006, ApJ, 646, 1098